Non-Prefabricated Nanocrystal Mesoporous TiO_2-Based Photoanodes Tuned by A Layer-by-Layer and Rapid Thermal Process

Junchao Tao, Yan Sun, Meiying Ge, Xin Chen,* and Ning Dai*

National Laboratory for Infrared Physics, Shanghai Institute of Technical Physics, Chinese Academy of Sciences, Shanghai 200083, China

ABSTRACT We describe a flexible and competent solution for fabrication of non-prefabricated nanocrystal mesoporous TiO_2-based photoanodes whose thicknesses are tunable from several hundreds of nanometers up to 12.4 μm. The combination of rapid thermal process and layer-by-layer spin-coating is successfully used to manipulate the structure and morphology of non-prefabricated nanocrystal mesoporous TiO_2 films. The photovoltaic performances of mesoporous TiO_2-based dye-sensitized solar cells depended on the thickness and the annealing temperature of mesoporous photoanodes. We systematically investigated and noted that the non-prefabricated nanocrystal mesoporous TiO_2 films ~6.3 μm thick annealed at 500 °C displayed better features in the short-circuit current density and overall conversion efficiency of mesoporous TiO_2-based dye-sensitized solar cells.

KEYWORDS: TiO_2 • mesoporous structure • non-prefabricated nanocrystal photoanode • dye-sensitized solar cells • layer-by-layer coating • rapid thermal process

1. INTRODUCTION

Depending on low cost and environmental compatibility, TiO_2-based photoanode materials have attracted great attention in energy conversion devices such as dye-sensitized solar cells (DSSCs) (1–7). In the past decades, TiO_2-based photoanodes were mainstream and almost based on the prefabricated TiO_2 nanocrystals in DSSCs. Recently, TiO_2 micro/nanostructures (e.g., TiO_2 tubes and mesopores) have been successfully applied as the photoanodes (8–10). In particular, the non-prefabricated nanocrystal mesoporous TiO_2 films have been one promising alternative photoanode candidate because of its large surface area, good grain contact, uniform mesopores, excellent mechanical stability, and tight adhesion on the substrates (11–13). All these characteristics are advantageous in light harvesting, electron transfer, and electrolyte diffusion in DSSCs (14–17). As for fabrication, the evaporation-induced self-assembly (EISA) process, a classical method for synthesizing mesoporous films, has been implemented for preparing mesoporous TiO_2-based photoanodes without a prefabricated-nanocrystal procedure (18–28). However, in a typical EISA process, a uniform layer of only ~300−500 nm thick takes more than 48 h. To the best of our knowledge, there are few reports on how to prepare and tune non-prefabricated nanocrystal mesoporous TiO_2-based photoanodes and improve the time/thickness efficiency by a simple and flexible process.

In this paper, we report the preparation and tuning of non-prefabricated nanocrystal mesoporous TiO_2-based photoanodes. By using a practicable non-prefabricated-nanocrystal procedure combining rapid thermal process and layer-by-layer spin-coating, we flexibly prepared and tuned mesoporous TiO_2 films up to ~12 μm in thickness within 16 h. The photovoltaic properties of non-prefabricated nanocrystal mesoporous TiO_2-based DSSCs are then investigated by tuning the thickness and annealing temperature of the mesoporous TiO_2 films.

2. EXPERIMENTAL SECTION

Preparation of Non-Prefabricated Crystal Mesoporous TiO_2 Films. Mesoporous TiO_2 films were prepared according to the following procedure. Typically, 3.0 mL concentrated hydrochloric (HCl, 36.5%) were added to 5 mL titanium tetraisopropoxide (abbreviated as TTIP) at room temperature under vigorous stirring. Then, 1.3 g of triblock copolymer P123 (Aldrich) dissolved in 15 mL of ethanol was added to the above solution of HCl/TTIP. The mixed solution was subsequently stirred for about 3 h at room temperature. Each mesoporous TiO_2 layer was obtained by spin-coating (2000 rpm, 20 s) the fresh precursor solution onto the precleaned conductive fluorine doped tin oxide (FTO) glass, followed by a rapid thermal process at 400 °C for 5 min and a cooling process at ambient temperature. The film thicknesses were adjusted by the cycle times of spin-coating and rapid thermal process. Finally, the films were calcined at 400−550 °C for 2 h.

Characterization of Mesoporous TiO_2 Films. X-ray diffraction (XRD) patterns were recorded on Rigaku D/max 2550 diffractometer using a high-power Cu Kα source operating at 40 kV and 150 mA. Scanning electron microscopy (SEM) images were obtained on FEI Sirion200 SEM with an accelerating voltage of 15 kV. Nitrogen adsorption/desorption isotherms were recorded on a Micromeritics ASAP 2400 nitrogen adsorption apparatus, for which the mesoporous TiO_2 films were scraped from FTO glass.

* Corresponding author. E-mail: xinchen@mail.sitp.ac.cn (X.C.); ndai@mail.sitp.ac.cn (N.D.).

Received for review October 6, 2009 and accepted November 30, 2009

DOI: 10.1021/am9006726

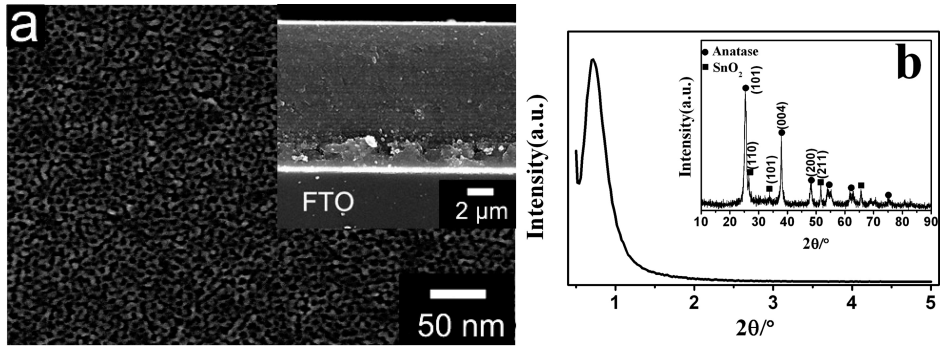

FIGURE 1. (a) SEM images of surface and cross-section (the inset) of non-prefabricated nanocrystal mesoporous TiO_2 films prepared by 35 cycles on FTO glass; (b) small- and wide-angle XRD patterns of mesoporous TiO_2 films on FTO glass.

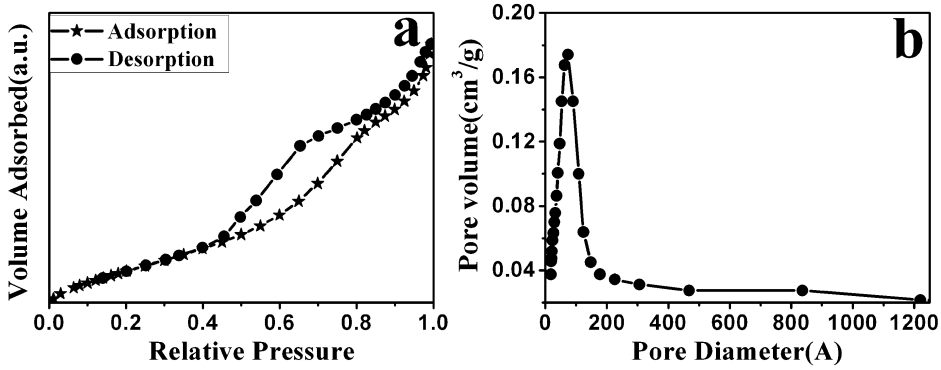

FIGURE 2. The plots for(a) N_2 adsorption/desorption isotherms and (b) BJH pore size distribution of non-prefabricated nanocrystal mesoporous TiO_2 films.

Preparation and Characterization of Mesoporous TiO_2-Based DSSCs. As-prepared mesoporous TiO_2 films were heated at 70 °C for 1 h, and then immersed in a 5×10^{-4} M ethanol solution of N719 ($RuL_2(NCS)_2$/2TBA, L = 2,2′-bipyridyl-4,4′-dicarboxylic acid, TBA = tetrabutylammonium) dye for 24 h. The photoanodes were air-dried at room temperature after being rinsed with ethanol to remove excess dye on the surface. The TiO_2 electrode absorbing N719 and a counterelectrode with Pt films of ~100 nm thick were assembled and sealed into a sandwich type cell with Dupont Surlyn 1702 (25 μm). The electrolyte was employed a solution of 0.6 M BMII (1-butyl-3-methylimidazolium iodide), 0.1 M I_2, 0.1 M LiI, and 0.5 M 4-tertbutylpyridine in acetonitrile. The absorption spectra of mesoporous TiO_2 films sensitized with N719 were recorded on Perkin-Elemer Lambda 2S spectrophotometer by using blank FTO glass as baseline. The irradiation source for the photocurrent−voltage (I−V) measurement is an AM 1.5 solar simulator (16S-002, Solar Light Co. Ltd., USA). The incident light intensity was 100 mW/cm^2 calibrated with a standard Si solar cell. The current−voltage curves were obtained by the linear sweep voltammetry (LSV) method using an electrochemical workstation (LK9805, Tianjing Lanlike Co., China). The measurement of incident photon-to-current conversion efficiency (IPCE) was performed by a Hypermonolight (SM-25, Jasco Co. Ltd., Japan).

3. RESULTS AND DISCUSSION

The non-prefabricated nanocrystal mesoporous TiO_2 films were prepared using a layer-by-layer cycle process by combining spin-coating and rapid thermal procedures on clean FTO substrates. The SEM images in Figure 1a shows the presence of mesopores in the TiO_2 films. Herein, the mesoporous TiO_2 film of ~10.8 μm thick (the inset in Figure 1a) was obtained by repeating 35 cycles of spin-coating and rapid thermal processes followed by a final heating procedure at 500 °C for 2 h. During the rapid thermal process at 400 °C, self-assembled copolymers (e.g., P123) were removed, and a crystalline TiO_2 framework with pores in nanometer scale then formed. As implied in Figure 1a, we can obtain mesoporous films 7−9 nm in size. It seems that the order of the mesoporous films was not as perfect as the one via EISA process (28, 29). However, the relatively high annealing temperature of about 500 °C and rapid thermal process in our case should be taken into account. The small-angle XRD pattern in Figure 1b shows a sharp diffraction peak at $2\theta \approx 0.72°$. This confirms the presence of the mesoporous structure. The well resolved peaks in wide-angle XRD pattern (the inset in Figure 1b) are indexed into (101), (004), (200), etc., attributing to diffraction peaks of anatase TiO_2. The average crystallite size is ~16 nm, as determined from (101) diffraction peak using Scherrer equation. Mesoporous structures in the as-prepared TiO_2 thick films were further verified by the N_2 adsorption and desorption method. Panels a and b in Figure 2 show the plots for N_2 adsorption/desorption isotherms and BJH pore size distribution of mesoporous TiO_2 films, respectively. The data imply the BET surface area of ~112 m^2/g with a pore volume of ~0.33 cm^3/g and an average pore diameter of ~8 nm. This further verifies the mesoprous structures and morphologies in TiO_2 films. The large surface area is helpful for the absorbance of dye and thus improve the short-circuit current density and conversion efficiency of TiO_2-based DSSCs.

As mentioned above, we can tune mesoporous TiO_2 films from hundreds of nanometers to tens of micrometers in thickness by varying cycle time and spin-coating rate. Figure

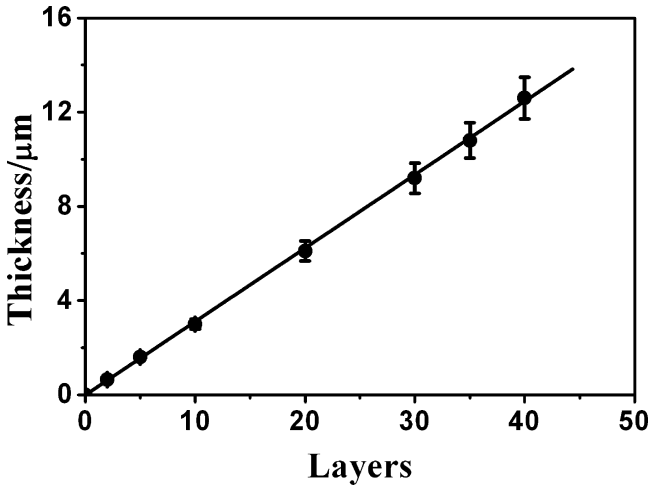

FIGURE 3. Plot of the film thickness and the layer number.

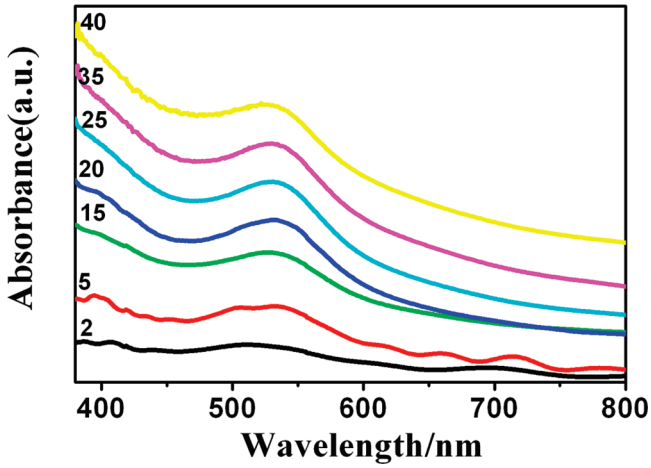

FIGURE 4. Absorption spectra of non-prefabricated nanocrystal mesoporous TiO_2 films sensitized with N719 with different cycle layers. Here, mesoporous films were first immersed in a 5×10^{-4} M solution of N719 in ethanol for 24 h.

3 shows the relationship between the total film thickness and cycle numbers. All thicknesses are derived from the cross-section SEM images of the mesoporous TiO_2 films after annealing at 500 °C for 2 h. It is obvious that the film thickness increases linearly with cycle numbers, and the linear slope of ~0.31. This implies that the thickness of each layer is ~0.31 μm, in agreement with SEM measurement. For example, a procudure of 40 cycle-times produced a film of ~12.4 μm thick. It is also important for the film thickness to adjust the rate of spin-coating and the viscosity of liquid precursor. In our case, we spent less than 16 h to obtain a film of ~12.4 μm thick. In contrast, it takes more than 3 days to achieve several μm thick TiO_2 films homemade in a typical EISA process. Hence, our method provides a facile and fast tuning of mesoporous TiO_2 films thickness, so that the time/thickness efficiency is dramatically improved.

Figure 4 shows the absorption spectra of mesoporous films of 2- to 40-layer thick films. In all cases, the mesoporous films were first immersed in a 5×10^{-4} M solution of N719 in ethanol. It can be seen that all spectra cover nearly the whole visible region. The relative absorbance intensities increase almost linearly with the thickness of films, resulting from the linear increase in the content of N719 dye absorbed in the films with the increase in film thickness. All these will help for photocurrent response at a wide spectrum scale.

These non-prefabricated nanocrystal mesoporous TiO_2 films are available and competent in DSSCs by tuning the thickness and morphology, as shown in Figures 5 and 6. Panels a and b in Figure 5 display the typical incident photon-to-current conversion efficiency (IPCE) spectrum and $I-V$ curve of non-prefabricated nanocrystal mesoporous TiO_2-based photoanodes (20 layers, ~6.3 μm thick) when N719 was used. A wide spectrum range for photocurrent response is observed in consistent with absorption spectra of mesoporous TiO_2 photoanodes sensitized with dye. The primary cell possesses a short-circuit current density of 13.2 mA cm^{-2}, an open-circuit voltage of 640 mV, a fill factor of 0.652, and a light conversion efficiency of ~5.51 % under a simulated AM 1.5 illumination. The selected active areas of solar cells were about 0.159 cm^{-2}. It is found that the short-circuit current density and conversion efficiency also depend on the thickness of mesoporous TiO_2-based photoanodes as implied in panels c and d in Figure 5. Both the conversion efficiency and short-circuit current density increase with film thickness up to 20 layers (~6.3 μm), and then decrease at the range from 20 layers to 35 layers. The variation in conversion efficiency and photocurrent density may be related to the electron photogeneration, transfer, and recombination. An increase in photoanode thickness directly increases the inner surface area, leading to higher loading amount of dye. Therefore, a thicker photoanode can absorb more photons for improving the light harvesting efficiency, resulting in higher photocurrent density and conversion efficiency. On the other hand, thicker photoanode also yields more recombination centers and longer electron transfer path that may in turn increase electron recombination and loss. This may explain the decrease in photocurrent density and conversion efficiency for much thicker films above 20 layers. Therefore, the conversion efficiency and short-circuit current density increase as the thickness up to 20 layers, and then begin to decrease when the thicknesses were further increased, as shown in panels c and d in Figure 5.

We also investigated the dependence of the photovoltaic performances of DSSCs on the annealing temperature of non-prefabricated nanocrystal mesoporous TiO_2-based photoanodes. The annealing temperature affected the mesoporous microstructure and then the performances of TiO_2-based photoanodes (30–32). The structure of mesoporous TiO_2 materials strongly depended on the annealing temperature according to wide-angle and small-angle XRD data presented in Figures S2 and S3 in the Supporting Information (33, 34). As confirmed in Figure S4 in the Supporting Information, the surface area decreased with the annealing temperature increase because of the growth in crystallites and variation in mesoporous structure to some degree. The peaks of anatase phase in wide-angle XRD became shaper and stronger with enhanced annealing temperature from 400 to 550 °C. This resulted from the increase of average crystallite size and degree of crystallinity. The small-angle

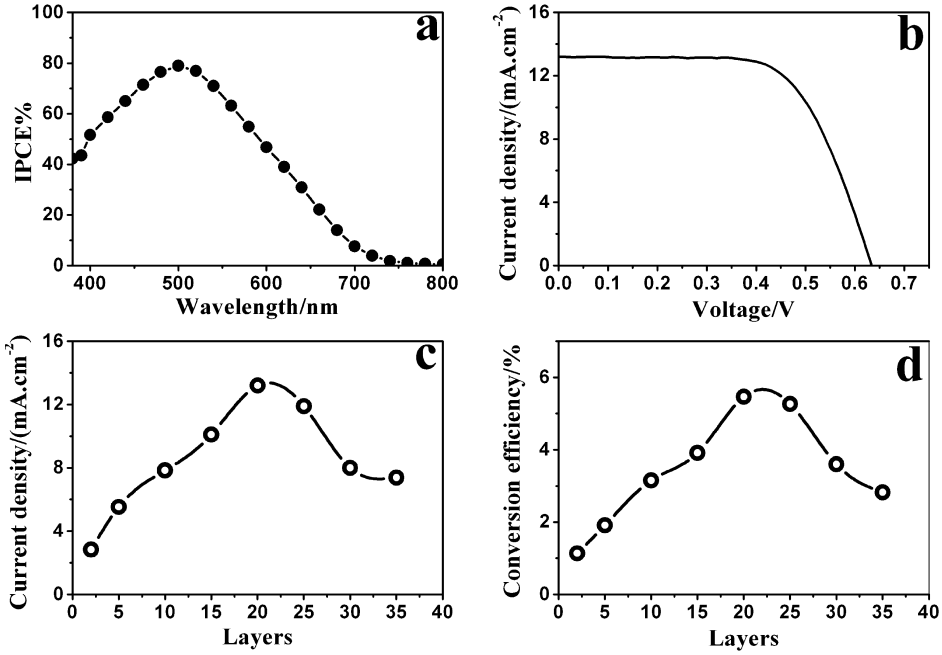

FIGURE 5. Photocurrent−voltage ($I-V$) measurements of non-prefabricated nanocrystal mesoporous TiO_2-based DSSCs under illumination of simulated AM 1.5 solar light (100 mW cm^{-2}): (a) IPCE characteristics when using 20 layers (~6.3 μm) as photoanode and N719 as dye; (b) $I-V$ curve when using 20 layers (~6.3 μm) as photoanode and N719 as dye; (c) the dependence of short-circuit current density on layer number; (d) conversion efficiency on layer number. Here, mesoporous photoanodes were annealed at 500 °C for 2 h.

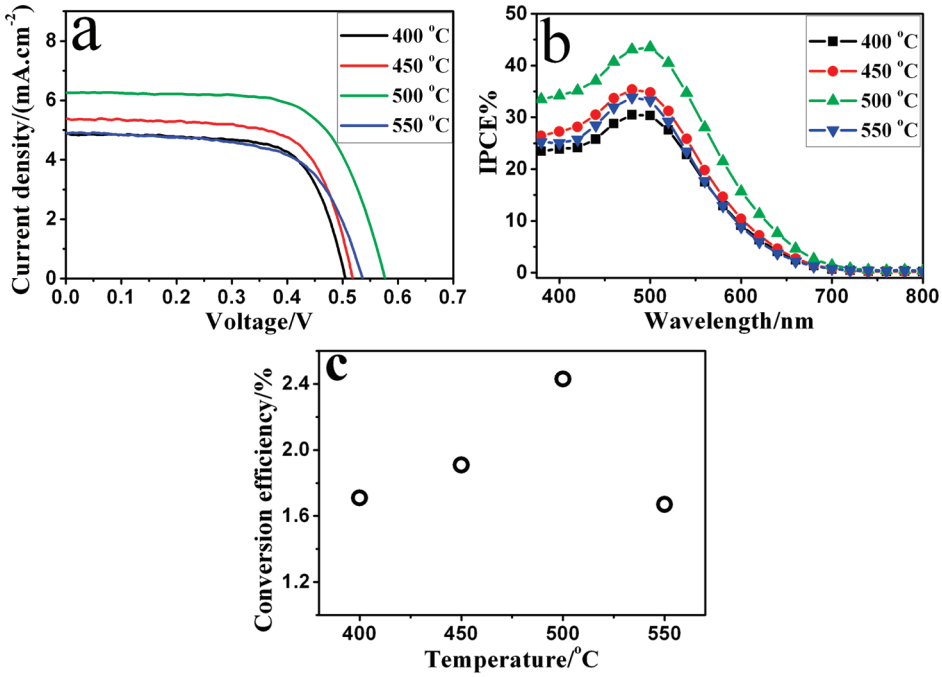

FIGURE 6. (a) $I-V$ measurements of non-prefabricated nanocrystal mesoporous TiO_2-based DSSCs with different photoanodes under illumination of simulated AM 1.5 solar light (100 mW cm^{-2}); (b) IPCE spectra of mesoporous-TiO_2-based DSSCs; (c) conversion efficiencies of mesoporous TiO_2-based DSSCs. In these cases, all films were prepared by 5 cycles on FTO glass and then annealed at 400, 450, 500, and 550 °C for 2 h, respectively.

XRD data imply that the films maintained mesoporous structure after annealed 400−500 °C. However, the diffraction peak in the small degrees disappeared after the film was annealed at 550 °C. This may be related to the damage and great variation in mesoporous structures at relatively higher temperature.

Figure 6 shows the $I-V$ curves, IPCE spectra, and conversion efficiencies of non-prefabricated nanocrystal mesoporous TiO_2-based photoanodes with N719. The photoanodes were prepared on FTO glass by 5 cycles and then annealed at 400, 450, 500, and 550 °C, respectively. The short-circuit current density first increases up to 500 °C, and then decrease beyond 500 °C. The IPCE spectra exhibit a similar trend. The conversion efficiency increase from 1.71 % at 400 °C to 2.43 % at 500 °C, and then decreased to 1.67 % at 550 °C. All these imply that the photoanodes annealed at 500

°C is more benefit to mesoporous TiO_2-based DSSCs. At 400 °C, mesoporous photoanodes maintain large surface area and can absorb more dye molecules (seen in Figure S4 in the Supporting Information). However, the films have a low degree of anatase crystallinity and thus possess quantities of surface states. Therefore, photoexcited electron can not be effective injected into the conduction band of TiO_2 and electron transfer in photoanode would be hindered. At 550 °C, with the coarsening of TiO_2 crystallites, the mesoporous structure maybe partly damaged (seen in small-angle XRD of Figure S3 in the Supporting Information), and the surface area of photoanodes strongly decreased (see Figure S4 in the Supporting Information). Lower surface area means a lower absorption amount of dye molecules, resulting in lower light harvesting efficiency and then photovoltaic performance. Furthermore, annealing temperature also plays an important role in the conductivity and light transmittance (see Figure S5 in the Supporting Information) of the substrate used as a current collector.

4. CONCLUSION

In summary, we have demonstrated the preparation and tuning of robust mesoporous-TiO_2-based photoanodes by combining layer-by-layer spin-coating and rapid thermal processes without a prefabricated nanocrystal procedure. The film thickness can be adjusted from several hundred nanometers up to 12.4 μm. Non-prefabricated nanocrystal mesoporous TiO_2 films have been used as the photoanodes, and the thickness and morphology dependence of cell photovoltaic performances were systematically studied. In our experiments, the non-prefabricated crystal mesoporous TiO_2 films of ~6.3 μm thick annealed at 500 °C displayed better features in DSSCs. We expect that the mesoporous TiO_2-based DSSCs can be further improved by optimizing the structures and morphologies of photoanodes, as well as the device structures (e.g., adding compact interlayer and light-scattering layer) (35–38).

Acknowledgment. This work is funded by National Basic Research Program of China (No. 2010CB933700), NSFC (No. 20704042), 863 (No.2009AA03Z412), and the Knowledge Innovation Program of CAS (No. KSCX2-YW-G-042)..

Supporting Information Available: XRD, UV—vis spectra, and $I-V$ of non-prefabricated nanocrystal mesoporous TiO_2-based films by tuning thickness and annealing temperature (PDF). This material is available free of charge via the Internet at http://pubs.acs.org.

REFERENCES AND NOTES

(1) Grätzel, M. *Nature* **2001**, *414*, 338.
(2) Grätzel, M. *Inorg. Chem.* **2005**, *44*, 6841.
(3) Hamann, T. W.; Jensen, R. A.; Martinson, A. B. F.; Ryswyk, H. V.; Hupp, J. T. *Energy Environ. Sci.* **2008**, *1*, 66.
(4) Ito, S.; Murakami, T. N.; Comte, P.; Liska, P.; Grätzel, C.; Nazeeruddin, M. K.; Grätzel, M. *Thin Solid Films* **2008**, *516*, 4613.
(5) Chiba, Y.; Islam, A.; Watanabe, Y.; Komiya, R.; Koide, N.; Han, L. *Jpn. J. Appl. Phys.* **2006**, *45*, L638.
(6) Chiba, Y.; Islam, A.; Komiya, R.; Koide, N.; Han, L. *Appl. Phys. Lett.* **2006**, *88*, 223505.
(7) Iwamoto, S.; Sazanami, Y.; Inoue, M.; Inoue, T.; Hoshi, T.; Shigaki, K.; Kaneko, M.; Maenosono, A. *ChemSusChem* **2008**, *1*, 401.
(8) Mor, G. K.; Shankar, K.; Paulose, M.; Varghese, O. K.; Grimes, C. A. *Nano Lett.* **2006**, *6*, 215.
(9) Meng, Q. B.; Fu, C. H.; Einaga, Y.; Gu, Z. Z.; Fujishima, A.; Sato, O. *Chem. Mater.* **2002**, *14*, 83.
(10) Law, M.; Greene, L. E.; Johnson, J. C.; Saykally, R.; Yang, P. D. *Nat. Mater.* **2005**, *4*, 455.
(11) Zukalova, M.; Zukal, A.; Kavan, L.; Nazeeruddin, M. K.; Liska, P.; Grätzel, M. *Nano Lett.* **2005**, *5*, 1789.
(12) Chen, D. H.; Huang, F. Z.; Cheng, Y. B.; Caruso, R. A. *Adv. Mater.* **2009**, *21*, 1.
(13) Beltran, E. L.; Prene, P.; Boscher, C.; Belleville, P.; Buvat, P.; Lambert, S.; Guillet, F.; Boissiere, C.; Grosso, D.; Sanchez, C. *Chem. Mater.* **2006**, *18*, 6152.
(14) Wei, M.; Konishi, Y.; Zhou, H.; Yanagida, M.; Sugihara, H.; Arakawa, H. *J. Mater. Chem.* **2006**, *16*, 1287.
(15) Ahn, K. S.; Kang, M. S.; Lee, J. W.; Kang, Y. S. *J. Appl. Phys.* **2007**, *101*, 084312.
(16) Kartini, I.; Menzies, D.; Blake, D.; Costa, J. C. D.; Meredith, P.; Richesd, J. D.; Lu, G. Q. *J. Mater. Chem.* **2004**, *14*, 2917.
(17) Kim, Y. J.; Lee, Y. H.; Lee, M. H.; Kim, H. J.; Pan, J. H.; Lim, G. I.; Choi, Y. S.; Kim, K.; Park, N. G.; Lee, C.; Lee, W. I. *Langmuir* **2008**, *24*, 13225.
(18) Ngamsinlapasathian, S.; Pavasupree, S.; Suzuki, Y.; Yoshikawa, S. *Sol. Energy Mater. Sol. Cells* **2006**, *90*, 3187.
(19) Hou, K.; Tian, B.; Li, F.; Bian, Z.; Zhao, D.; Huang, C. *J. Mater. Chem.* **2005**, *15*, 2414.
(20) Zukalova, M.; Prochazka, J.; Zukal, A.; Yum, J. H.; Kavan, L. *Inorg. Chim. Acta* **2008**, *361*, 656.
(21) Chen, W.; Sun, X.; Cai, Q.; Weng, D.; Li, H. *Electrochem. Commun.* **2007**, *9*, 382.
(22) Nedelcu, M.; Lee, J.; Crossland, E. J. W.; Warren, S. C.; Orilall, M. C.; Guldin, S.; Huttner, S.; Ducati, C.; Eder, D.; Wiesner, U.; Steiner, U.; Snaith, H. J. *Soft Matter* **2009**, *5*, 134.
(23) Chi, B.; Zhao, L.; Li, J.; Pu, J.; Chen, Y.; Wu, C. C.; Jin, T. *J. Nanosci. Nanotechnol.* **2008**, *8*, 3877.
(24) Wang, Y. Q.; Chen, S. G.; Tang, X. H.; Palchik, O.; Zaban, A.; Koltypin, Y.; Gedanken, A. *J. Mater. Chem.* **2001**, *11*, 521.
(25) Wan, Y.; Yang, H. F.; Zhao, D. *Acc. Chem. Res.* **2006**, *39*, 423.
(26) Wu, C. W.; Ohsuna, T.; Kuwabara, M.; Kuroda, K. *J. Am. Chem. Soc.* **2006**, *128*, 4544.
(27) Crepaldi, E. L.; Soler-Illia, G. J; de, A. A.; Grosso, D.; Cagnol, F.; Ribot, F.; Sanchez, C. *J. Am. Chem. Soc.* **2003**, *125*, 9770.
(28) Choi, S. Y.; Mamak, M.; Coombs, N.; Chopra, N.; Ozin, G. A. *Adv. Funct. Mater.* **2004**, *14*, 335.
(29) Liu, K.; Fu, H.; Shi, K.; Xiao, F.; Jing, L.; Xin, B. *J. Phys. Chem. B* **2005**, *109*, 18719.
(30) Zhao, D.; Peng, T. Y.; Lu, L. L.; Cai, P.; Jiang, P.; Bian, Z. Q. *J. Phys. Chem. C* **2008**, *112*, 8486.
(31) Nakade, S.; Matsuda, M.; Kambe, S.; Saito, Y.; Kitamura, T.; Sakata, T.; Wada, Y.; Mori, H.; Yanagida, S. *J. Phys. Chem. B* **2002**, *106*, 10004.
(32) Prochazka, J.; Kavan, L.; Shklover, V.; Zukalova, M.; Frank, O.; Kalbac, M.; Zukal, A.; Pelouchova, H.; Janda, P.; Mocek, K.; Klementova, M.; Carbone, D. *Chem. Mater.* **2008**, *20*, 2985.
(33) Phonthammachai, N.; Chairassameewong, T.; Gulari, E.; Jamieson, A. M.; Wongkasemjit, S. *Microporous Mesoporous Mater.* **2003**, *66*, 261.
(34) Yu, J.; Yu, J. C.; Ho, W.; Leung, M. K. P.; Cheng, B.; Zhang, G.; Zhao, X. *Appl, Catal. A* **2003**, *255*, 309.
(35) Chou, T. P.; Zhang, Q. F.; Russo, B.; Fryxell, G. E.; Cao, G. *J. Phys. Chem. C* **2007**, *111*, 6296.
(36) Fattakhova-Rohlfing, D.; Wark, M.; Brezesinski, T.; Smarsly, B. M.; Rathousky, J. *Adv. Funct. Mater.* **2007**, *17*, 123.
(37) Burke, A.; Ito, S.; Snaith, H.; Bach, U.; Kwiatkowski, J.; Grätzel, M. *Nano Lett.* **2008**, *8*, 977.
(38) Ito, S.; Liska, P.; Comte, P.; Charvet, R.; Pechy, P.; Bach, U.; Schmidt-Mende, L.; Zakeeruddin, S. M.; Kay, A.; Nazeeruddin, M. K.; Grätzel, M. *Chem. Commun.* **2005**, 4351.

AM9006726